

Interface-Controlled Conductive Fibers for Wearable Strain Sensors and Stretchable Conducting Wires

Zherui Cao,^{†,‡} Ranran Wang,^{*,†} Tengyu He,^{†,‡} Fangfang Xu,^{†,‡} and Jing Sun^{*,†}

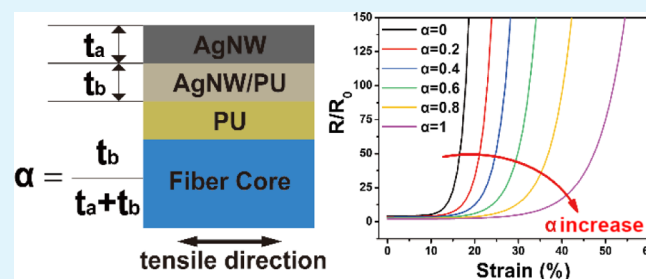
[†]State Key Laboratory of High Performance Ceramics and Superfine Microstructure, Shanghai Institute of Ceramics, Chinese Academy of Sciences, 1295 Ding Xi Road, Shanghai 200050, P. R. China

[‡]University of Chinese Academy of Sciences, 19 Yuquan Road, Beijing 100049, P. R. China

S Supporting Information

ABSTRACT: As an important subfield of flexible electronics, conductive fibers have been an active area of research. The interfacial interaction between nanostructured conductive materials with elastic substrates plays a vital role in the electromechanical performance of conductive fibers. However, the underlying mechanism has seldom been investigated. Here, we propose a fabricating strategy for a silver nanowire (Ag NW)/polyurethane composite fiber with a sheath-core architecture. The interfacial bonding layer is regulated, and its influence on the performance of conductive fibers is investigated, based on which an interfacial interaction model is proposed. The model underlines the significance of the embedding depth of the Ag NW network. Both supersensitive (gauge factor up to 9557) and ultrastable (negligible conductance degradation below the strain of 150%) conductive fibers are obtained via interface regulating, exhibiting great potential in the applications of wearable sensors and stretchable conducting connections.

KEYWORDS: interface control, silver nanowire, conductive fiber, wearable sensor, stretchable connection



1. INTRODUCTION

Flexible electronics with rapid development are desirable for next-generation applications, such as artificial skins,^{1–8} smart prosthetics,^{9–11} human-activity monitoring,^{12–19} and personal healthcare.^{20–25} Conductive fibers, as an important subfield of flexible electronics, have been an active area of research because of the significant potential for developing lightweight, flexible, and stretchable electronic devices on textile products.^{26–29} Conventional conductive fibers based on metal wires cannot conform well to human bodies, restricted by their poor mechanical compliance.^{30,31} In the past decade, conductive fibers consisted of elastic polymer substrates and nanostructured conductive materials such as silver nanowires (Ag NWs),^{32–34} copper nanowires,^{35,36} carbon nanotubes (CNTs),^{37–39} graphene,^{40,41} and metal nanoparticles^{42,43} have integrated various novel properties, such as high mechanical strength, structural flexibility, and electrical conductivity.

Generally, various approaches to prepare conductive fibers can be grouped into two categories. One approach exploits the incorporation of conductive filler materials into a polymer matrix through blending. Ma et al. fabricated highly conductive stretchable fibers by a scalable wet spinning process using flower-shaped silver nanoparticles (Ag NPs) (Ag nanoflowers) and polyurethane (PU).⁴⁴ The fibers could be made into ropes and fabric to improve the electromechanical performance, and no obvious resistance increase of weft-knitted fabric occurred under 200% strain. Lee et al. synthesized a highly stretchable conductive fiber through embedding Ag NWs and Ag NPs into

a styrene–buta–diene–styrene elastomeric matrix.⁴⁵ Because of the large amount of the conductive fillers and the high elasticity of the elastomer matrix, the Ag NW-embedded fiber exhibited superior initial electrical conductivity and stretch limit. In the other approach, conductive fibers are fabricated by modifying the surface of conventional fibers with novel functional materials. Liu et al. fabricated highly stretchable sheath-core conducting fibers by wrapping CNT sheets on prestrained rubber fiber cores.⁴⁶ The fiber enabled a resistance variation of less than 5% at a strain of 1000% because of its buckling structure in both the axial and belt directions. Cheng et al. developed a graphene-based composite fiber sensor with a “compression spring” structure by a coating method, featuring the ability of monitoring multiple kinds of deformation.⁴⁷ In the two categories, the conductive fibers often own a large area of interfaces between nanostructured conductive materials with elastic substrates.^{48,49} When subjected to stretching, the interfacial microstructure and its change determine the mechanical and electrical properties of the conductive fibers.^{50,51} Nonetheless, few researchers have paid attention to clarifying the underlying mechanism of interactions between the conductive materials and the stretchable substrates, which significantly influence the electromechanical performance of the conductive fibers.

Received: December 27, 2017

Accepted: April 3, 2018

Published: April 3, 2018

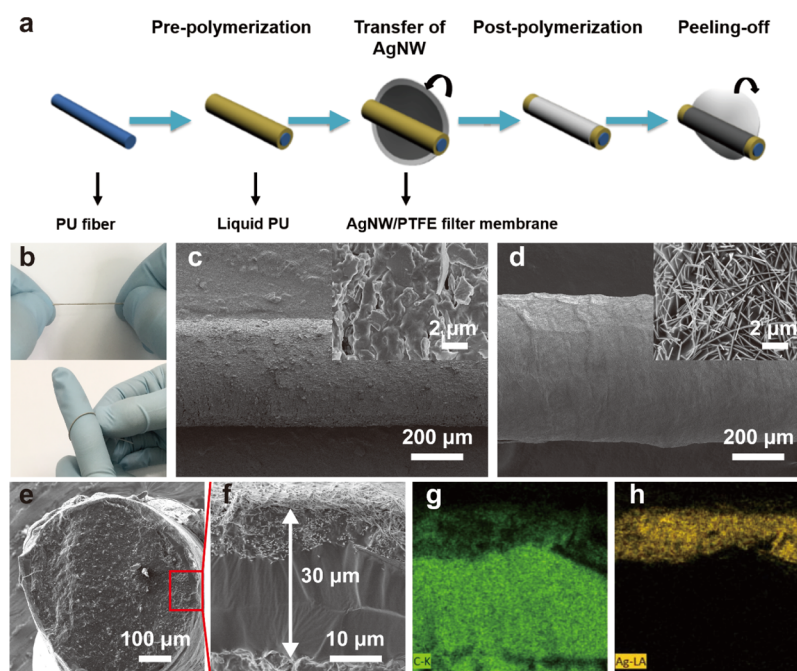


Figure 1. (a) Schematic illustration of the fabrication of the Ag NW/PU fiber. (b) Upper photograph shows the as-prepared Ag NW/PU fiber. The lower photograph demonstrates the Ag NW/PU fiber winding around a finger. (c) SEM images of the bare PU fiber. (d) SEM images of the as-prepared Ag NW/PU fiber. (e,f) SEM images of the cross section of the as-prepared Ag NW/PU fiber. (g,h) Energy-dispersive spectrometry (EDS) mapping of the Ag NW/PU fiber to demonstrate the distribution of C and Ag.

Herein, we proposed a facial fabricating strategy for a Ag NW/PU composite fiber with a sheath-core architecture. We introduced a bonding layer with tunable stickiness to combine PU cores and Ag NW films and to adjust the interfacial adhesion and the microstructure of the fibers. Through the interface regulating, conductive fibers with quite opposite electromechanical performance were obtained. In one case, the fiber exhibited significant resistance variation versus strain, with a high sensitivity [gauge factor (GF) up to 9557], as well as a large response range (60%), ultralow detection limit ($<0.1\%$ strain), and excellent reliability and durability ($>10\,000$ cycles), indicating its great potential for applications in wearable strain sensors. While in the other case, the fiber showed insignificant conductivity decrease at the high deformation level. Stretchable conducting wires with an initial resistance lower than $1\,\Omega\cdot\text{cm}^{-1}$ and relative resistance change lower than 10% under the strain of 110% were fabricated. The interfacial microstructure and its change under different strain were characterized to disclose the underlying mechanism. An interfacial interaction model was proposed based on the electromechanical test, which shed new light on the influence of the bonding layer. The model may inspire novel interfacial designs of stretchable electronics. Furthermore, monitoring of human physiological signals and motions, as well as dynamic infrared (IR) thermal measurement was carried out to demonstrate the practical applications of this conductive fiber with tunable functions.

2. RESULTS AND DISCUSSION

2.1. Fabrication and Characterization of the Ag NW/PU Fibers. Figure 1a illustrates the schematic fabrication process of the Ag NW/PU fiber. Initially, Ag NWs were collected on a polytetrafluoroethylene (PTFE) filter membrane through vacuum filtration. Liquid PU as the bonding layer was coated onto a bare PU fiber, followed by precuring at $80\,^{\circ}\text{C}$ for a period of time until a sticky PU layer formed. Then, the Ag

NW/PTFE filter membrane was wrapped around the core fiber tightly, and it was fully postpolymerized at $80\,^{\circ}\text{C}$ for 3 h. Finally, the Ag NW/PU fiber was prepared after peeling off the PTFE filter membrane. The length of the fibers might be restricted by the size of the filter membranes. To increase the length of the conductive fibers, a press-and-roll process can be utilized to transfer conductive materials (see the [Supporting Information](#) for details). The as-prepared Ag NW/PU fiber was flexible enough to conform to arbitrary curved surfaces, such as a human finger (Figure 1b), indicating its possible application in wearable electronics. Figure 1c and the inset present the scanning electron microscopy (SEM) images of the bare PU fiber.

The PU fiber (diameter of $500\,\mu\text{m}$) serves as a highly flexible and stretchable core of the conductive fiber. Through the adhesion of the interfacial PU layer, homogeneous Ag NW films attached tightly onto the core PU fiber. As shown in Figure 1d, the surface of the Ag NW/PU fiber is smooth and compact, without any cracks or fractures. The nanowires overlapped randomly with no orientation. The mechanical properties of the Ag NW/PU composite fiber and PU are shown in Figure S1. It can be found that the Ag NWs/PU composite fiber gives a mechanical response similar to that of the pure PU substrate. The PU and Ag NW/PU fibers ruptured at a strain close to 1000% (998 and 980%, respectively). The tensile strength values of the PU and Ag NW/PU fibers are 36.99 and 38.24 MPa, respectively. We speculated that the Ag NW and PU layers on the fiber core hardened the composite fiber, which decreased the limit strain. Figure 1e–h represents the cross-sectional SEM and EDS mapping images of the Ag NW/PU fiber, confirming the homogeneity of the sheath layer with the thickness of about $30\,\mu\text{m}$.

2.2. Electromechanical Properties of the Ag NW/PU Fibers. During the transfer process, the liquid PU with low viscosity penetrated into the Ag NW network, resulting in the

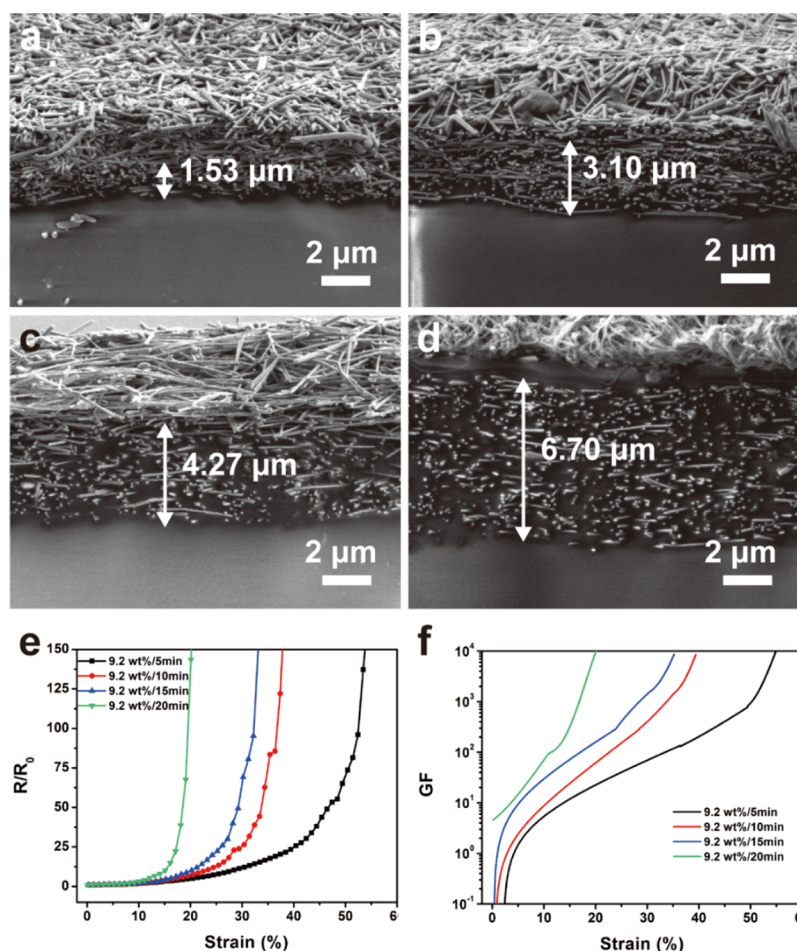


Figure 2. (a–d) Cross-sectional SEM images of the Ag NW/PU-9.2 wt %/20 min (a), Ag NW/PU-9.2 wt %/15 min (b), Ag NW/PU-9.2 wt %/10 min (c), and Ag NW/PU-9.2 wt %/5 min (d) fibers. (e) Resistance variation vs strain of the Ag NW/PU fibers with different prepolymerization time from 5 to 20 min (stretching rate of 1% strain per second). (f) GFs vs strain of the Ag NW/PU fibers with different prepolymerization time.

embedding of the Ag NWs. This embedding process played an important role in the attachment of the Ag NWs to the PU substrate. Figure 2a–d shows the cross-sectional SEM images of the Ag NW/PU fibers with different prepolymerization time from 5 to 20 min. The amount of Ag NWs of all the samples was 1 mL. For the fibers fabricated with 0.5, 1, 1.5, and 2 mL Ag NWs, the mass fractions of Ag NWs are 5.4, 9.2, 13.1, and 16.7%, respectively. The embedding depth of the Ag NWs increased with the shortening of the prepolymerization time. This is because with prolonging of the prepolymerization time, more and more oligomers cross-linked and were not able to penetrate into the Ag NW network. When the prepolymerization time was prolonged to 20 min, most of the Ag NWs stacked on the top of the PU substrate with an embedding depth of only 1.53 μm (Figure 2a). On the contrary, a prepolymerization time of 5 min led to a stickier and softer PU interfacial layer, which brought in deeper embedding of the Ag NW network with a depth of about 6.7 μm. The initial conductivity of these fibers increased from 159.73 to 240.36 S·cm⁻¹ along with the decreased embedding depth from 6.7 to 1.53 μm (Table S1, Supporting Information). Figure 2e exhibits the resistance variation versus strain of the Ag NW/PU fibers with different prepolymerization time. The resistance variation (R/R_0) of the four samples monotonically increased with the applied strain, in an approximately exponential fashion. Furthermore, we found that there is a trade-off between the

sensitivity and stretchability with regard to the prepolymerization time. The R/R_0 increased faster for the fibers with longer prepolymerization time, while the sensing range of the fibers extended as the prepolymerization time decreased. From the curve of the resistance variation, we can obtain the GF of the fiber, which is defined as $(R - R_0)/R_0/\epsilon$, where ϵ is the strain. GFs as a function of strain for the four fibers are plotted in Figure 4f. All the four samples showed highly sensitivity to deformation. For the Ag NW/PU-9.2 wt %/20 min fiber, the averaged GF is from 5 to 96 for the strain range within 11% and 96 to 9557 for 11–20%, which is appropriate for high GF with low strain sensors. In contrast, the Ag NW/PU-9.2 wt %/5 min fiber possesses a GF from 0.1 to 118 for the strain range within 35% and 118 to 940 for 35–50%, indicating the potential to be utilized for strain sensors with both high GF and large working range. We also fabricated fibers with different amounts of Ag NWs to explore influence of thickness of the Ag NWs on the performance. With the prepolymerization time fixed, the Ag NW film got thicker with the increased amount of Ag NWs, as shown in Figure S2. Figure S3 exhibits the resistance variation versus strain of the fibers with different amounts of Ag NWs. The resistances change less at large strains for the fibers with thicker Ag NW films.

2.3. Analysis and Modeling of the Interfacial Interaction of the Ag NW/PU Fibers. An interfacial interaction model of the Ag NW/PU composite fiber was

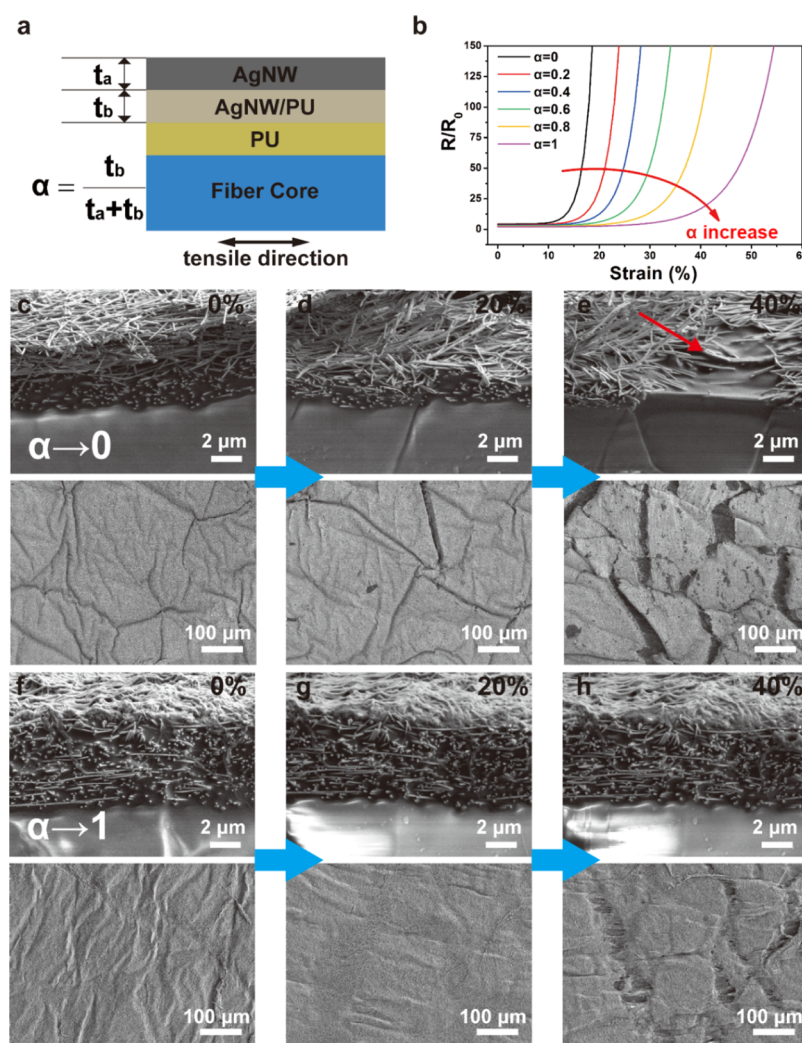


Figure 3. (a) Schematic illustration of the longitudinal section of the Ag NW/PU fiber. (b) Modeling of the resistance variation vs strain of the Ag NW/PU fibers with different interface bonding strengths. (c–h) Longitudinal section and top view SEM images of the Ag NW/PU-9.2 wt %/20 min (c–e) and Ag NW/PU-9.2 wt %/5 min (f–h) fibers at the strain from 0 to 40%.

proposed to illustrate the effect of the bonding layer on the conductive fiber. As shown in Figure 3a, the fiber is mainly composed of four layers, including the fiber core, PU layer, Ag NW/PU composite layer, and unembedded Ag NW layer, among which the top two layers would mainly determine the resistance variation with strain. With the amount of Ag NWs fixed, the thickness of each layer is dependent on the prepolymerization time. Many complex physical factors which affect the performance of the composite fiber are hard to quantify. Therefore, we define α as the thickness ratio of the embedding Ag NWs to the whole Ag NWs

$$\alpha = \frac{t_b}{t_a + t_b} \quad (1)$$

Here, t_a and t_b are the thickness of the Ag NW/PU composite layer and unembedded Ag NW layer, respectively (the physical meaning of α is given in the Supporting Information).

We assume the 9.2 wt %/20 min and 9.2 wt %/5 min as the unembedded and fully embedded conditions, respectively. For the Ag NW/PU-9.2 wt %/20 min fiber, most of the Ag NWs stack on top of the PU substrate, where α is close to 0. In contrast, for the Ag NW/PU-9.2 wt %/5 min fiber, the Ag NW

network is almost completely buried into the sticky and soft PU substrate, where α is close to 1. On the basis of the electromechanical test of the fibers (Figure 2e), the sensing mode satisfies the exponential expression. Thus, we have

$$\alpha \rightarrow 0, \quad \frac{R}{R_0} = A_1 \cdot \exp(B_1 \cdot \varepsilon) + C_1 \quad (2)$$

$$\alpha \rightarrow 1, \quad \frac{R}{R_0} = A_2 \cdot \exp(B_2 \cdot \varepsilon) + C_2 \quad (3)$$

Here A_1 , A_2 , B_1 , B_2 , C_1 , and C_2 are constants (Table S2, Supporting Information). They are used to represent the effects of the physical factors in the system to make the mechanism analysis more concise and intuitional.

In the partly embedded conditions, α varies from 0 to 1 with different prepolymerization time. The resistance variation could be written as

$$0 < \alpha < 1, \quad \frac{R}{R_0} = A \cdot \exp(B \cdot \varepsilon) + C \quad (4)$$

Because the electromechanical performance of the fiber is simultaneously affected by the Ag NW/PU composite layer and the unembedded Ag NW layer, the constants are correlated

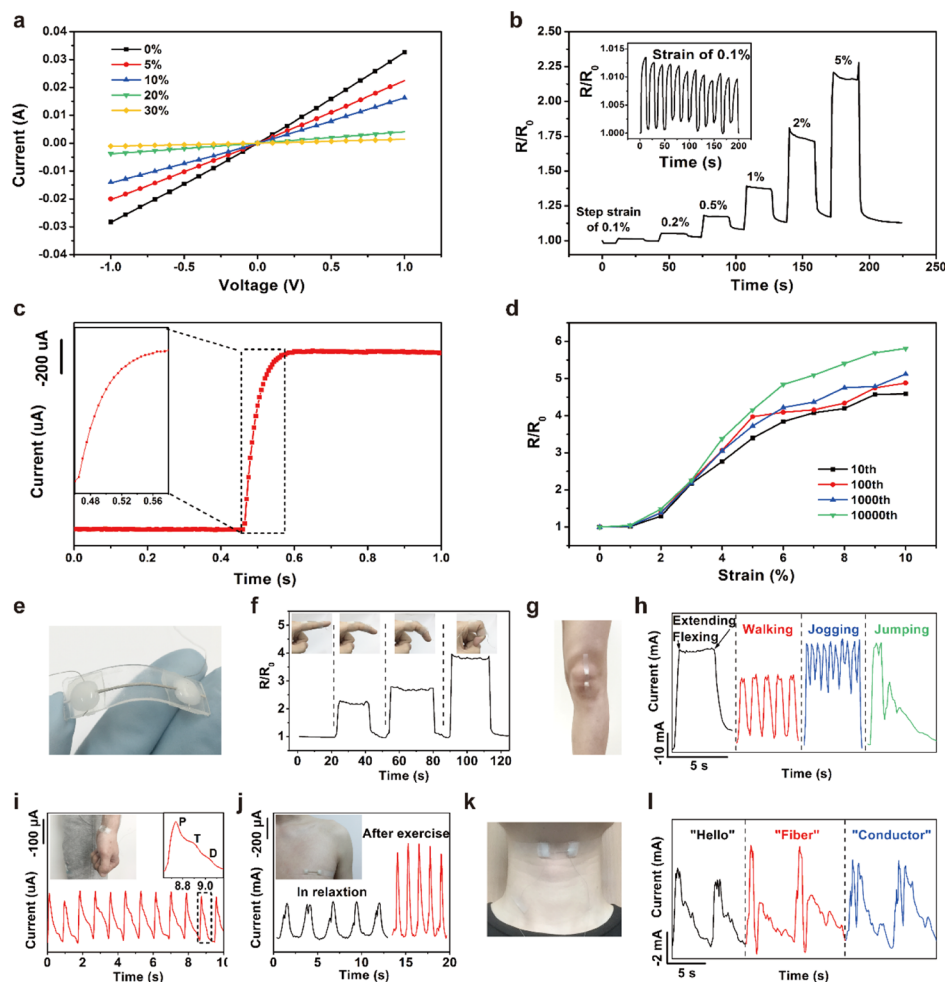


Figure 4. (a) Current–voltage curves of the Ag NW/PU fiber at different strains. (b) Resistance variation under step strains from 0.1 to 5%. The inset shows the output signal at consecutive input step strain of 0.1%. (c) Current signal of the Ag NW/PU fiber to a quasi-transient input strain of 0.5%. Inset: closeup of the response time (resolution limit of 5 ms). (d) Resistance variation during cycle tests: 10th (black), 100th (red), 1000th (blue), and 10 000th (green) cycles at the strain from 0 to 10%. (e) Photograph of the wearable sensor. (f) Response signal of the wearable sensor in monitoring finger-bending. Inset: photographs of finger-bending at increasing angles. (g) Wearable sensor attached to the knee. (h) Responsive curves of the wearable sensor on the knee under motions of flexing/extending, walking, jogging, and jumping. (i) Responsive curves of the wearable sensor on the wrist. Insets: photograph and the measured profile. (j) Responsive curves of the wearable sensor on the chest in relaxation and after exercise. (k) Wearable sensor attached to the throat. (l) Responsive curves when the wearer spoke “hello”, “fiber”, and “conductor”.

with the thickness ratio α . On the basis of the mixed model theory, linear and log-linear mixed models are used to predict the values of the constants. According to the linear mixed model, we have the following relations

$$A_1 = (1 - \alpha) \cdot A_1 + \alpha \cdot A_2 \quad (5)$$

$$B_1 = (1 - \alpha) \cdot B_1 + \alpha \cdot B_2 \quad (6)$$

$$C_1 = (1 - \alpha) \cdot C_1 + \alpha \cdot C_2 \quad (7)$$

According to the log-linear mixed model, we have the following relations

$$\ln A_{1-1} = (1 - \alpha) \cdot \ln A_1 + \alpha \cdot \ln A_2 \quad (8)$$

$$\ln B_{1-1} = (1 - \alpha) \cdot \ln B_1 + \alpha \cdot \ln B_2 \quad (9)$$

$$\ln C_{1-1} = (1 - \alpha) \cdot \ln C_1 + \alpha \cdot \ln C_2 \quad (10)$$

To try the best to calculate the values of A , B , and C accurately, we have

$$A = \sqrt{A_1 \times A_{1-1}} \quad (11)$$

$$B = \sqrt{B_1 \times B_{1-1}} \quad (12)$$

$$C = \sqrt{C_1 \times C_{1-1}} \quad (13)$$

Through substituting the values in eq 4, we can calculate the constants under different embedding conditions and speculate the model of the resistance versus strain. As plotted in Figure 3b, the fiber exhibits lower sensitivity and larger working range as α increases. This variation trend is consistent with the electromechanical test (Figure 2e). We can provide a quantitative understanding of the influence of each layer or set the thickness ratio based on the desired performance of the fiber as shown in Figure 4.

The microstructure variation of the fibers at different stretching stages was characterized to disclose the underlying mechanism. Figure 3c–e shows the longitudinal section and the top view SEM images of the Ag NW/PU-9.2 wt %/20 min fiber at the strain from 0 to 40%. The Ag NWs randomly stacked on the surface of the PU substrate with a limited embedded depth

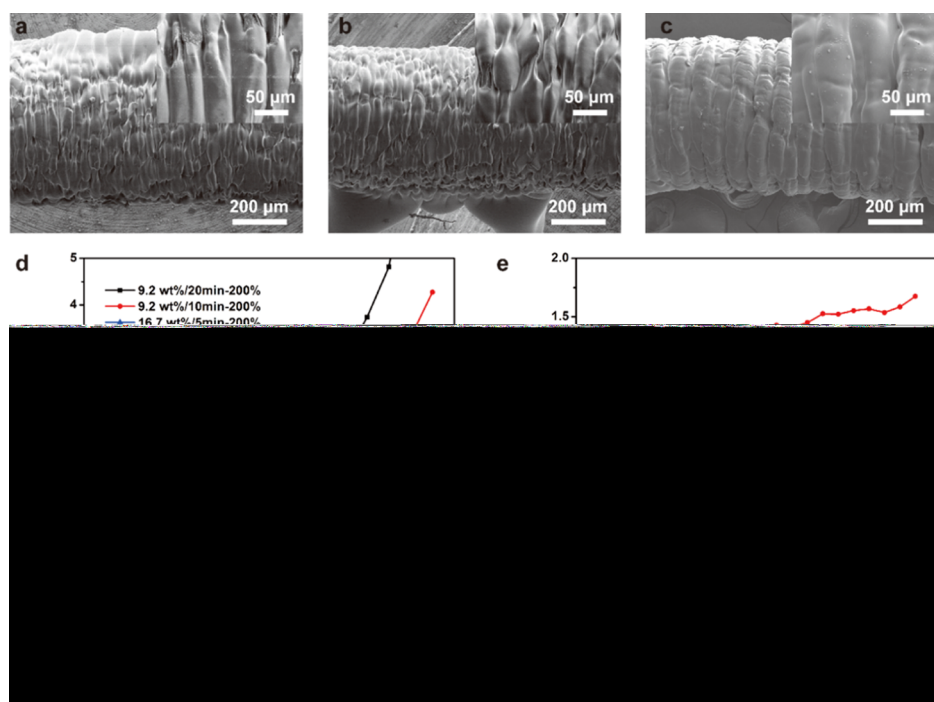


Figure 5. (a–c) SEM images of surface microstructure morphology of the PU/Ag NW/PU-9.2 wt %/20 min (a), PU/Ag NW/PU-9.2 wt %/10 min (b), and PU/Ag NW/PU-16.7 wt %/5 min (c) fibers. (d) Resistance variation vs strain of the PU/Ag NW/PU-9.2 wt %/20 min, PU/Ag NW/PU-9.2 wt %/10 min, and PU/Ag NW/PU-16.7 wt %/5 min fibers. (e) Resistance variation of the PU/Ag NW/PU-16.7 wt %/5 min fiber as a function of 10 000 stretching/releasing cycles at a strain of 50 and 100%. (f) IR thermal images of PU/Ag NW/PU-16.7 wt %/5 min fiber at different stretching stages from strains of 0–150%.

(Figure 3c). When stretched to 20%, the Ag NW network slid by the deformation of the fiber core. The displacement of Ag NWs developed into cracks in the stress concentration area, causing the rapid increase of resistance (Figure 3d). When stretched to 40%, the cracks continued growing and led to obvious fracture in both the unembedded Ag NW layer and the Ag NW/PU composite layer, which destroyed the conductive network. On the contrary, no obvious destruction was observed when stretched to 40% from the longitudinal section SEM image of the Ag NW/PU-9.2 wt %/5 min fiber (Figure 3f–h). From the top view SEM image of Figure 3h, we can find some cracks on the surface of the unembedded layer, while the embedded part still kept sufficient conductive paths. Unlike the random stack of Ag NWs in the unembedded layer of Ag NW/PU-9.2 wt %/20 min, obvious alignment of Ag NWs along the stretch direction was observed in the fiber of Ag NW/PU-9.2 wt %/5 min, which can be attributed to the strong interaction between Ag NWs and PU substrates (Figure S6). It is believed that the alignment of the nanowires with stretch would help keep the integrity of the conducting paths, which explained the extended working range.

2.4. Ag NW/PU Fibers as Wearable Strain Sensors. To balance the sensitivity and stretchability of the fibers, we chose the Ag NW/PU-9.2 wt %/10 min fibers as strain sensors for the measurement and demonstration of the sensing properties. Figure 4a shows the current–voltage characteristics of an Ag NW/PU fiber under different strains. The fiber exhibited an ohmic behavior in spite of applied strains, and the current monotonically declined with the increase of the strain. Step strains were applied to determine the detection limit of the fiber sensor (Figure 4b). The detection limit could be as minute as 0.1% for the high sensitivity under small deformation, and the output signal was highly reproducible at minute strains

(inset in Figure 4b). To investigate the response time, the sensor was loaded with a quasi-transient step strain of 0.5%. As plotted in the high-resolution $I-t$ signal curve (Figure 4c), the response time was determined to be about 120 ms. Figure 4d presents the durability test results of 10 000 cyclic stretching (0 to 10% strain). The signal curve remained nearly invariable within 1000 cycles. After 100 and 1000 cycles, the relative signal drifts at the strain of 10% of the fiber were only 29.4 and 53.1%, respectively, showing the reliability for the practical application as daily wearable sensors.

To demonstrate the potential of Ag NW/PU fibers as wearable sensors, the fiber was assembled onto an ultrathin polydimethylsiloxane (PDMS) film, which could be compressed on the human skin with the help of medical tape (Figure 4e). In vigorous motion capturing, the wearable sensors were attached onto the knuckle (inset in Figure 4f) and the knee (Figure 4g). Figure 4f shows that the sensor could respond to the bending of an index finger, indicating its potential application as gesture remote. Figure 4h presents the monitoring of physical activities of legs. Various motions such as extending/flexing, walking, jogging, and jumping could be differentiated by the corresponding curves, suggesting the possible utilization in the digital training of athletics. To detect subtle physiological signals, we fixed the wearable sensors to the wrist, chest, and throat (Figure 4i–k). The detection of pulse and respiration change is indispensable for some illness diagnoses. As presented in Figure 4i, the output signal displayed a matching waveform with distinguishable percussion, tidal, and diastolic peaks of the human pulse. Figure 4j shows the excellent performance of the sensor for respiration measurement. Different rates and depths of respiration could be monitored in relaxation and after exercise. As shown in Figure 4l, the sensor exhibited voice recognition capabilities

when the wearer spoke different words, such as “hello”, “fiber”, and “conductor”. The full-range detection of human activities of the sensor indicates its great potential for applications in personal healthcare and human–machine interactions.

2.5. Ag NW/PU Fibers as Stretchable Conducting Wires. In addition to strain sensors, another favorable application of the conductive fibers is the stretchable conductor. The prestrain-then-buckling process is commonly used in the fabrication of stretchable conductors.^{52,53} Here, we found that the prepolymerization time would influence the buckling structure and the corresponding electromechanical performance of the Ag NW/PU fibers. The fabrication process was similar to that illustrated in Figure 1a, except that the core PU fiber was prestretched to 200% before the transfer of the Ag NW film. Another difference was that the Ag NW/PU fiber was treated with H₂ plasma to improve the conductivity of the network (Figure S7). As reported by Wang et al.,⁵⁴ Ag NWs were wrapped by residual organics and oxide layers which decreased the conductive paths in the network before H₂ plasma treatment. The etching and reductive effects of H₂ plasma could remove these layers. And the photothermal effect was enhanced at the contact points of nanowires because of the surface plasmonic resonance effect, which contributed to the local nanowelding. Besides, the Ag NW film was encapsulated by a thin layer of PU before prestrain release to avoid the axial cracking due to radial expansion during the release process (Figure S8).

The obtained conductive fibers exhibited a resistance lower than 1 $\Omega\cdot\text{cm}^{-1}$, rendering an outstanding conductivity among the nanomaterial-based stretchable conductors. Figure 5a–c shows the SEM images of surface morphology of the PU/Ag NW/PU fibers with different prepolymerization time. The PU/Ag NW/PU composite layer developed buckles in a uniform manner because of sufficient adhesion to the substrate, which prevented rupturing of the conductive pathways under large deformation. The height and width of the buckles increased when the fibers were fabricated with a short prepolymerization time and a large amount of Ag NWs. Figure S9 monitored the microstructure change on the surface of the PU/Ag NW/PU fibers when stretched to 100 and 200%. The buckles gradually flattened with increasing strain in all the three fibers to accommodate the deformation. Obvious cracks were observed in the PU/Ag NW/PU-9.2 wt %/20 min fiber at the strain of 100%. These cracks grew into obvious ruptures with further stretch, which led to significant increment in the resistance of the fiber, as shown in Figure 5d. By comparison, the PU/Ag NW/PU-9.2 wt %/10 min fiber did not show obvious rupture on the surface until 200% strain, resulting in enhanced electromechanical stability. The PU/Ag NW/PU-16.7 wt %/5 min fiber exhibited the minimum resistance variation versus strain because of the deeper and wider buckling structure as well as the thicker embedded nanowire network (large α as shown in Figure S10). The resistance variations at 50, 100, and 150% strain were 7.0, 9.5, and 52.5%, respectively, as obtained from Figure 5d. Figure 5e demonstrates the cycling performance of the PU/Ag NW/PU-16.7 wt %/5 min fiber. Upon stretching/releasing with a maximum strain of 50% for 10 000 cycles, the resistance of the PU/Ag NW/PU-200% fiber showed only a small increase of 14.8%. Further increasing the maximum stretching strain up to 100%, the resistance change of the fiber after 10 000 cycles was measured to be 67.4%, demonstrating a good electromechanical durability and stability. Compared with the previously reported highly conductive Ag/

PU fiber which underwent a dramatic decrease in conductivity at the high deformation level,⁴⁴ or the highly stretchable CNT based fiber with a large initial resistance,⁴⁶ our fiber exhibited a balanced conductivity and stability.

To demonstrate the potential of the conductive fibers for stretchable conducting wires, we took IR thermal images of the PU/Ag NW/PU-16.7 wt %/5 min fiber at different stretching stages (Figure 5f). The fiber was stretched up to 150% strain at a constant dc voltage (1 V), and no obvious temperature variation was observed, showing its outstanding stretchability and stability under tensile strain, which is promising for the applications of stretchable conducting connections and wearable heaters.

3. CONCLUSIONS

In summary, we presented an interface-controlled Ag NW/PU composite fiber. Through introducing a bonding layer between the conductive material and the stretchable substrate, we explained the effect of the interfacial interaction and adjusted sensitivity and stretchability of the fibers aiming at applications from wearable strain sensors to stretchable conducting wires. As strain sensors, the fibers with different GFs and working ranges can be prepared to the need of individual utilization, which are appropriate for monitoring full-range human motions. On the contrary, the fibers with prestrain show insignificant conductivity decay under large tensile strain, which can be ideal connections for flexible circuits. Furthermore, the fabrication strategy can be extended to other flexible electronics with diverse materials for the precise control of the interface and performance.

4. EXPERIMENTAL SECTION

4.1. Fabrication of the Ag NW/PU Fiber. First, Ag NW suspensions (10 mg/mL, from Zhejiang Kechuang Advanced Materials Co., Ltd.) were filtrated to form films on PTFE filter membranes (diameter of 47 mm, pore size of 220 nm). A bare PU fiber (diameter of $\sim 500\ \mu\text{m}$, commercially available) was dipcoated with a thin layer of liquid PU (ratio of the prepolymer to the chain extender, 10:4 by mass, from Shanghai Haksong of Polymer Science and Technology Co., Ltd.). Then, the fiber was kept at 80 $^{\circ}\text{C}$ for 5–20 min to form a thin layer of precured PU on the surface of the core fiber. Afterward, the Ag NW/PTFE film was wrapped around the fiber tightly with the Ag NWs side facing the PU layer. Ag NWs were transferred to the fiber surface with the aid of the stickiness of the precured PU. The PU on the surface of the fiber was completely cured after a postpolymerization process (80 $^{\circ}\text{C}$ for 3 h). Finally, the Ag NW/PU fiber was prepared after peeling off the PTFE filter membrane.

4.2. Integration of the Ag NW/PU Fiber into Wearable Sensors. The Ag NW/PU fiber (4 cm in length) was put onto a PDMS (a 10:1 mixture of the PDMS prepolymer and the curing agent, Sylgard-184, Dow Corning) film (40 mm \times 10 mm \times 0.5 mm). Copper wires (2 μm in diameter) as electrodes were connected to the two ends of the fiber using conductive silver paste. Subsequently, the two ends of the fiber were fixed onto PDMS by coating RTV silicone rubber and curing at room temperature for 8 h. Finally, the wearable sensors were attached onto target positions of the body with the help of medical tape.

4.3. Fabrication of the PU/Ag NW/PU Fiber. First, Ag NW suspensions (10 mg/mL) were filtrated to form films on PTFE filter membranes (diameter of 47 mm, pore size of 220 nm). A bare PU fiber (diameter of $\sim 500\ \mu\text{m}$, commercially available) was stretched to strain of 200% and fixed. Then, the prestrained PU fiber was dipcoated with a thin layer of liquid PU (ratio of prepolymer to chain extender, 10:4 by mass). Then, the fiber was kept at 80 $^{\circ}\text{C}$ for 5–20 min to form a thin layer of precured PU on the surface of the core fiber. Afterward, the Ag NW/PTFE film was wrapped around the fiber tightly with the

Ag NWs side facing the PU layer. Ag NWs were transferred to the fiber surface with the aid of the stickiness of the precured PU. The PU on the surface of the fiber was completely cured after a postpolymerization process (80 °C for 3 h). Then, the fiber was treated in H₂ plasma for 5 min. After that, the fiber was coated with liquid PU, leaving the two ends naked for electric connection and kept at 80 °C for 2 h. Finally, the prestrain of the PU fiber was released to form a buckling microstructure on the surface of the fiber.

4.4. Characterization. The SEM and EDS characterization was accomplished using Hitachi SU4800 FE-SEM. In the test of the electromechanical properties, the strain loading was implemented with a high-precision motorized linear stage (displacement resolution of 2.5 μm). The real-time current signal was acquired using an electrochemical workstation (PARSTAT 2273, Princeton Applied Research). IR thermal images were obtained by an IR thermal camera.

■ ASSOCIATED CONTENT

● Supporting Information

The Supporting Information is available free of charge on the ACS Publications website at DOI: 10.1021/acsami.7b19699.

Press-and-roll process which can be utilized to prepare long conductive fibers, mechanical properties of the composite fiber and its substrate, cross-sectional SEM images of the fibers with different amounts of the Ag NWs, resistance variation versus strain of the fibers with different amounts of Ag NWs, physical meaning of α , SEM image of the alignment of Ag NWs along the stretch direction, SEM images of the Ag NW network after H₂ plasma treatment, effect of the encapsulation on the prestretched conductive fibers, morphology change of the surface buckling microstructure at different stretching stages from strains of 0–200%, thicker embedded nanowire network of the conductive fibers for stretchable wires, conductivities of the fibers with different prepolymerization time, and values of the constants in eqs 2 and 3 (PDF)

■ AUTHOR INFORMATION

Corresponding Authors

*E-mail: wangranran@mail.sic.ac.cn (R.W.).

*E-mail: jingsun@mail.sic.ac.cn (J.S.).

ORCID

Fangfang Xu: 0000-0002-5570-4289

Jing Sun: 0000-0003-1101-1584

Author Contributions

The manuscript was written through contributions of all authors. All authors have given approval to the final version of the manuscript.

Notes

The authors declare no competing financial interest.

■ ACKNOWLEDGMENTS

This work was financially supported by the Youth Innovation Promotion Association CAS (2014226), the Major State Research Development Program of China (2016YFA0203000), Shanghai Key Basic Research Project (16JC1402300), and Shanghai Science and Technology Rising Star Project (17QA1404700).

■ REFERENCES

- (1) Lee, S.-K.; Kim, B. J.; Jang, H.; Yoon, S. C.; Lee, C.; Hong, B. H.; Rogers, J. A.; Cho, J. H.; Ahn, J.-H. Stretchable graphene transistors with printed dielectrics and gate electrodes. *Nano Lett.* **2011**, *11*, 4642–4646.
- (2) Yeo, W.-H.; Kim, Y.-S.; Lee, J.; Ameen, A.; Shi, L.; Li, M.; Wang, S.; Ma, R.; Jin, S. H.; Kang, Z.; Huang, Y.; Rogers, J. A. Multifunctional Epidermal Electronics Printed Directly Onto the Skin. *Adv. Mater.* **2013**, *25*, 2773–2778.
- (3) Lee, J.-H.; Lee, K. Y.; Gupta, M. K.; Kim, T. Y.; Lee, D.-Y.; Oh, J.; Ryu, C.; Yoo, W. J.; Kang, C.-Y.; Yoon, S.-J.; Yoo, J.-B.; Kim, S.-W. Highly Stretchable Piezoelectric-Pyroelectric Hybrid Nanogenerator. *Adv. Mater.* **2014**, *26*, 765–769.
- (4) Koo, J. H.; Jeong, S.; Shim, H. J.; Son, D.; Kim, J.; Kim, D. C.; Choi, S.; Hong, J.-I.; Kim, D.-H. Wearable Electrocardiogram Monitor Using Carbon Nanotube Electronics and Color-Tunable Organic Light-Emitting Diodes. *ACS Nano* **2017**, *11*, 10032–10041.
- (5) Xu, S.; Zhang, Y.; Jia, L.; Mathewson, K. E.; Jang, K.-I.; Kim, J.; Fu, H.; Huang, X.; Chava, P.; Wang, R. H.; Bhole, S.; Wang, L.; Na, Y. J.; Guan, Y.; Flavin, M.; Han, Z.; Huang, Y.; Rogers, J. A. Soft Microfluidic Assemblies of Sensors, Circuits, and Radios for the Skin. *Science* **2014**, *344*, 70–74.
- (6) Trung, T. Q.; Ramasundaram, S.; Hwang, B.-U.; Lee, N.-E. An All-Elastomeric Transparent and Stretchable Temperature Sensor for Body-Attachable Wearable Electronics. *Adv. Mater.* **2016**, *28*, 502–509.
- (7) Chen, D.; Pei, Q. Electronic Muscles and Skins: A Review of Soft Sensors and Actuators. *Chem. Rev.* **2017**, *117*, 11239–11268.
- (8) Yokota, T.; Zalar, P.; Kaltenbrunner, M.; Jinno, H.; Matsuhisa, N.; Kitanosako, H.; Tachibana, Y.; Yukita, W.; Koizumi, M.; Someya, T. Ultraflexible organic photonic skin. *Sci. Adv.* **2016**, *2*, e1501856.
- (9) Son, D.; Lee, J.; Qiao, S.; Ghaffari, R.; Kim, J.; Lee, J. E.; Song, C.; Kim, S. J.; Lee, D. J.; Jun, S. W.; Yang, S.; Park, M.; Shin, J.; Do, K.; Lee, M.; Kang, K.; Hwang, C. S.; Lu, N.; Hyeon, T.; Kim, D.-H. Multifunctional wearable devices for diagnosis and therapy of movement disorders. *Nat. Nanotechnol.* **2014**, *9*, 397–404.
- (10) Kim, J.; Lee, M.; Shim, H. J.; Ghaffari, R.; Cho, H. R.; Son, D.; Jung, Y. H.; Soh, M.; Choi, C.; Jung, S.; Chu, K.; Jeon, D.; Lee, S.-T.; Kim, J. H.; Choi, S. H.; Hyeon, T.; Kim, D.-H. Stretchable silicon nanoribbon electronics for skin prosthesis. *Nat. Commun.* **2014**, *5*, 5747.
- (11) Larson, C.; Peele, B.; Li, S.; Robinson, S.; Totaro, M.; Beccai, L.; Mazzolai, B.; Shepherd, R. Highly stretchable electroluminescent skin for optical signaling and tactile sensing. *Science* **2016**, *351*, 1071–1074.
- (12) Roh, E.; Hwang, B.-U.; Kim, D.; Kim, B.-Y.; Lee, N.-E. Stretchable, Transparent, Ultrasensitive, and Patchable Strain Sensor for Human-Machine Interfaces Comprising a Nanohybrid of Carbon Nanotubes and Conductive Elastomers. *ACS Nano* **2015**, *9*, 6252–6261.
- (13) Yamada, T.; Hayamizu, Y.; Yamamoto, Y.; Yomogida, Y.; Izadi-Najafabadi, A.; Futaba, D. N.; Hata, K. A stretchable carbon nanotube strain sensor for human-motion detection. *Nat. Nanotechnol.* **2011**, *6*, 296–301.
- (14) Yan, C.; Wang, J.; Kang, W.; Cui, M.; Wang, X.; Foo, C. Y.; Chee, K. J.; Lee, P. S. Highly stretchable piezoresistive graphene-nanocellulose nanopaper for strain sensors. *Adv. Mater.* **2014**, *26*, 2022–2027.
- (15) Wang, C.; Li, X.; Gao, E.; Jian, M.; Xia, K.; Wang, Q.; Xu, Z.; Ren, T.; Zhang, Y. Carbonized Silk Fabric for Ultrastretchable, Highly Sensitive, and Wearable Strain Sensors. *Adv. Mater.* **2016**, *28*, 6640–6648.
- (16) Liu, Q.; Chen, J.; Li, Y.; Shi, G. High-Performance Strain Sensors with Fish-Scale-Like Graphene-Sensing Layers for Full-Range Detection of Human Motions. *ACS Nano* **2016**, *10*, 7901–7906.
- (17) Amjadi, M.; Pichitpajongkit, A.; Lee, S.; Ryu, S.; Park, I. Highly Stretchable and Sensitive Strain Sensor Based on Silver Nanowire-Elastomer Nanocomposite. *ACS Nano* **2014**, *8*, 5154–5163.
- (18) Hu, C.; Li, Z.; Wang, Y.; Gao, J.; Dai, K.; Zheng, G.; Liu, C.; Shen, C.; Song, H.; Guo, Z. Comparative assessment of the strain-sensing behaviors of polylactic acid nanocomposites: reduced graphene oxide or carbon nanotubes. *J. Mater. Chem. C* **2017**, *5*, 2318–2328.

- (19) Huang, W.; Dai, K.; Zhai, Y.; Liu, H.; Zhan, P.; Gao, J.; Zheng, G.; Liu, C.; Shen, C. Flexible and Lightweight Pressure Sensor Based on Carbon Nanotube/Thermoplastic Polyurethane-Aligned Conductive Foam with Superior Compressibility and Stability. *ACS Appl. Mater. Interfaces* **2017**, *9*, 42266–42277.
- (20) Choong, C.-L.; Shim, M.-B.; Lee, B.-S.; Jeon, S.; Ko, D.-S.; Kang, T.-H.; Bae, J.; Lee, S. H.; Byun, K.-E.; Im, J.; Jeong, Y. J.; Park, C. E.; Park, J.-J.; Chung, U.-I. Highly stretchable resistive pressure sensors using a conductive elastomeric composite on a micropylramid array. *Adv. Mater.* **2014**, *26*, 3451–3458.
- (21) Wang, X.; Gu, Y.; Xiong, Z.; Cui, Z.; Zhang, T. Silk-molded flexible, ultrasensitive, and highly stable electronic skin for monitoring human physiological signals. *Adv. Mater.* **2014**, *26*, 1336–1342.
- (22) Webb, R. C.; Bonifas, A. P.; Behnaz, A.; Zhang, Y. H.; Yu, K. J.; Cheng, H.; Shi, M.; Bian, Z.; Liu, Z.; Kim, Y.-S.; Yeo, W.-H.; Park, J. S.; Song, J.; Li, Y.; Huang, Y.; Gorbach, A. M.; Rogers, J. A. Ultrathin conformal devices for precise and continuous thermal characterization of human skin. *Nat. Mater.* **2013**, *12*, 938–944.
- (23) Lee, H.; Song, C.; Hong, Y. S.; Kim, M. S.; Cho, H. R.; Kang, T.; Shin, K.; Choi, S. H.; Hyeon, T.; Kim, D.-H. Wearable/disposable sweat-based glucose monitoring device with multistage transdermal drug delivery module. *Sci. Adv.* **2017**, *3*, e1601314.
- (24) Rogers, J. A.; Someya, T.; Huang, Y. Materials and mechanics for stretchable electronics. *Science* **2010**, *327*, 1603–1607.
- (25) Miyamoto, A.; Lee, S.; Cooray, N. F.; Lee, S.; Mori, M.; Matsuhisa, N.; Jin, H.; Yoda, L.; Yokota, T.; Itoh, A.; Sekino, M.; Kawasaki, H.; Ebihara, T.; Amagai, M.; Someya, T. Inflammation-free, gas-permeable, lightweight, stretchable on-skin electronics with nanomeshes. *Nat. Nanotechnol.* **2017**, *12*, 907–913.
- (26) Zhong, J.; Zhang, Y.; Zhong, Q.; Hu, Q.; Hu, B.; Wang, Z. L.; Zhou, J. Fiber-Based Generator for Wearable Electronics and Mobile Medication. *ACS Nano* **2014**, *8*, 6273–6280.
- (27) Weng, W.; Sun, Q.; Zhang, Y.; Lin, H.; Ren, J.; Lu, X.; Wang, M.; Peng, H. Winding Aligned Carbon Nanotube Composite Yarns into Coaxial Fiber Full Batteries with High Performances. *Nano Lett.* **2014**, *14*, 3432–3438.
- (28) Seyedin, S.; Razal, J. M.; Innis, P. C.; Jeiranikhameneh, A.; Beirne, S.; Wallace, G. G. Knitted Strain Sensor Textiles of Highly Conductive All-Polymeric Fibers. *ACS Appl. Mater. Interfaces* **2015**, *7*, 21150–21158.
- (29) Zhu, S.; So, J.-H.; Mays, R.; Desai, S.; Barnes, W. R.; Pourdeyimi, B.; Dickey, M. D. Ultrastretchable Fibers with Metallic Conductivity Using a Liquid Metal Alloy Core. *Adv. Funct. Mater.* **2013**, *23*, 2308–2314.
- (30) Qiao, L.; Xiaoming, T. A stretchable knitted interconnect for three-dimensional curvilinear surfaces. *Text. Res. J.* **2011**, *81*, 1171–1182.
- (31) Wakuda, D.; Suganuma, K. Stretchable fine fiber with high conductivity fabricated by injection forming. *Appl. Phys. Lett.* **2011**, *98*, 073304.
- (32) Wei, Y.; Chen, S.; Yuan, X.; Wang, P.; Liu, L. Multiscale Wrinkled Microstructures for Piezoresistive Fibers. *Adv. Funct. Mater.* **2016**, *26*, 5078–5085.
- (33) Cheng, Y.; Wang, R.; Sun, J.; Gao, L. Highly Conductive and Ultrastretchable Electric Circuits from Covered Yarns and Silver Nanowires. *ACS Nano* **2015**, *9*, 3887–3895.
- (34) Gong, S.; Cheng, W. One-Dimensional Nanomaterials for Soft Electronics. *Adv. Electron. Mater.* **2017**, *3*, 1600314.
- (35) Won, Y.; Kim, A.; Yang, W.; Jeong, S.; Moon, J. A highly stretchable, helical copper nanowire conductor exhibiting a stretchability of 700%. *NPG Asia Mater.* **2014**, *6*, e132.
- (36) Cheng, Y.; Zhang, H.; Wang, R.; Wang, X.; Zhai, H.; Wang, T.; Jin, Q.; Sun, J. Highly Stretchable and Conductive Copper Nanowire Based Fibers with Hierarchical Structure for Wearable Heaters. *ACS Appl. Mater. Interfaces* **2016**, *8*, 32925–32933.
- (37) Ryu, S.; Lee, P.; Chou, J. B.; Xu, R.; Zhao, R.; Hart, A. J.; Kim, S.-G. Extremely Elastic Wearable Carbon Nanotube Fiber Strain Sensor for Monitoring of Human Motion. *ACS Nano* **2015**, *9*, 5929–5936.
- (38) Foroughi, J.; Spinks, G. M.; Aziz, S.; Mirabedini, A.; Jeiranikhameneh, A.; Wallace, G. G.; Kozlov, M. E.; Baughman, R. H. Knitted Carbon-Nanotube-Sheath/Spandex-Core Elastomeric Yarns for Artificial Muscles and Strain Sensing. *ACS Nano* **2016**, *10*, 9129–9135.
- (39) Zheng, Y.; Li, Y.; Li, Z.; Wang, Y.; Dai, K.; Zheng, G.; Liu, C.; Shen, C. The effect of filler dimensionality on the electromechanical performance of polydimethylsiloxane based conductive nanocomposites for flexible strain sensors. *Compos. Sci. Technol.* **2017**, *139*, 64–73.
- (40) Qu, G.; Cheng, J.; Li, X.; Yuan, D.; Chen, P.; Chen, X.; Wang, B.; Peng, H. A Fiber Supercapacitor with High Energy Density Based on Hollow Graphene/Conducting Polymer Fiber Electrode. *Adv. Mater.* **2016**, *28*, 3646–3652.
- (41) Yun, Y. J.; Hong, W. G.; Kim, W.-J.; Jun, Y.; Kim, B. H. A novel method for applying reduced graphene oxide directly to electronic textiles from yarns to fabrics. *Adv. Mater.* **2013**, *25*, 5701–5705.
- (42) Ma, R.; Lee, J.; Choi, D.; Moon, H.; Baik, S. Knitted fabrics made from highly conductive stretchable fibers. *Nano Lett.* **2014**, *14*, 1944–1951.
- (43) Lee, J.; Kwon, H.; Seo, J.; Shin, S.; Koo, J. H.; Pang, C.; Son, S.; Kim, J. H.; Jang, Y. H.; Kim, D. E.; Lee, T. Conductive fiber-based ultrasensitive textile pressure sensor for wearable electronics. *Adv. Mater.* **2015**, *27*, 2433–2439.
- (44) Ma, R.; Kang, B.; Cho, S.; Choi, M.; Baik, S. Extraordinarily High Conductivity of Stretchable Fibers of Polyurethane and Silver Nanoflowers. *ACS Nano* **2015**, *9*, 10876–10886.
- (45) Lee, S.; Shin, S.; Lee, S.; Seo, J.; Lee, J.; Son, S.; Cho, H. J.; Algadi, H.; Al-Sayari, S.; Kim, D. E.; Lee, T. Ag Nanowire Reinforced Highly Stretchable Conductive Fibers for Wearable Electronics. *Adv. Funct. Mater.* **2015**, *25*, 3114–3121.
- (46) Liu, Z. F.; Fang, S.; Moura, F. A.; Ding, J. N.; Jiang, N.; Di, J.; Zhang, M.; Lepro, X.; Galvao, D. S.; Haines, C. S.; Yuan, N. Y.; Yin, S. G.; Lee, D. W.; Wang, R.; Wang, H. Y.; Lv, W.; Dong, C.; Zhang, R. C.; Chen, M. J.; Yin, Q.; Chong, Y. T.; Zhang, R.; Wang, X.; Lima, M. D.; Ovalle-Robles, R.; Qian, D.; Lu, H.; Baughman, R. H. Hierarchically buckled sheath-core fibers for superelastic electronics, sensors, and muscles. *Science* **2015**, *349*, 400–404.
- (47) Cheng, Y.; Wang, R.; Sun, J.; Gao, L. A Stretchable and Highly Sensitive Graphene-Based Fiber for Sensing Tensile Strain, Bending, and Torsion. *Adv. Mater.* **2015**, *27*, 7365–7371.
- (48) Jiang, S.; Zhang, H.; Song, S.; Ma, Y.; Li, J.; Lee, G. H.; Han, Q.; Liu, J. Highly Stretchable Conductive Fibers from Few-Walled Carbon Nanotubes Coated on Poly(m-phenylene isophthalamide) Polymer Core/Shell Structures. *ACS Nano* **2015**, *9*, 10252–10257.
- (49) Ge, J.; Sun, L.; Zhang, F.-R.; Zhang, Y.; Shi, L.-A.; Zhao, H.-Y.; Zhu, H.-W.; Jiang, H.-L.; Yu, S.-H. A Stretchable Electronic Fabric Artificial Skin with Pressure-, Lateral Strain-, and Flexion-Sensitive Properties. *Adv. Mater.* **2016**, *28*, 722–728.
- (50) Park, J. J.; Hyun, W. J.; Mun, S. C.; Park, Y. T.; Park, O. O. Highly stretchable and wearable graphene strain sensors with controllable sensitivity for human motion monitoring. *ACS Appl. Mater. Interfaces* **2015**, *7*, 6317–6324.
- (51) Wang, R.; Jiang, N.; Su, J.; Yin, Q.; Zhang, Y.; Liu, Z.; Lin, H.; Moura, F. A.; Yuan, N.; Roth, S.; Rome, R. S.; Ovalle-Robles, R.; Inoue, K.; Yin, S.; Fang, S.; Wang, W.; Ding, J.; Shi, L.; Baughman, R. H.; Liu, Z. A Bi-Sheath Fiber Sensor for Giant Tensile and Torsional Displacements. *Adv. Funct. Mater.* **2017**, *27*, 1702134.
- (52) Lee, P.; Lee, J.; Lee, H.; Yeo, J.; Hong, S.; Nam, K. H.; Lee, D.; Lee, S. S.; Ko, S. H. Highly stretchable and highly conductive metal electrode by very long metal nanowire percolation network. *Adv. Mater.* **2012**, *24*, 3326–3332.
- (53) Yu, J.; Lu, W.; Pei, S.; Gong, K.; Wang, L.; Meng, L.; Huang, Y.; Smith, J. P.; Booksh, K. S.; Li, Q.; Byun, J.-H.; Oh, Y.; Yan, Y.; Chou, T.-W. Omnidirectionally Stretchable High-Performance Supercapacitor Based on Isotropic Buckled Carbon Nanotube Films. *ACS Nano* **2016**, *10*, S204–S211.
- (54) Wang, R.; Zhai, H.; Wang, T.; Wang, X.; Cheng, Y.; Shi, L.; Sun, J. Plasma-induced nanowelding of a copper nanowire network and its

application in transparent electrodes and stretchable conductors. *Nano Res.* **2016**, 9, 2138–2148.